ORIGINAL PAPER: SOL–GEL, HYBRIDS, AND SOLUTION CHEMISTRIES

Check for updates

# Amylases immobilization by sol–gel entrapment: application for starch hydrolysis

José Rodrigo Fernandez Caresani[1] · Alexsandro Dallegrave[2] · João H. Z. dos Santos[2]

Abstract

α-amylase from *Bacillus subtilis*, α-amylase from *Aspergillus oryzae*, and β-amylase from barley were encapsulated within silica-based matrix by acid-catalyzed sol–gel process. The resulting systems were characterized by Fourier transform infrared spectroscopy (FT-IR) in the attenuated total reflection (ATR) mode, nitrogen adsorption (BET and BJH methods), scanning electron microscopy (SEM), and small-angle X-ray scattering (SAXS). The products from enzymatic hydrolysis of starch were analyzed by the DNS method (reducing sugars) and high-performance liquid chromatography (HPLC). The biocatalytic activity of the immobilized systems (reducing sugars in the range of 0–30.5 µmol/mL) was compared with that of the free systems (reducing sugars in the range of 11.7–33.7 µmol/mL). The porosity analysis showed that xerogels with a high surface area (above 300 m^2/g) were obtained. The morphological analyses carried out by microscopy demonstrated the existence of predominantly granular (relatively spherical particles) structures. HPLC results show large differences in the musts obtained from the free enzymes and the corresponding immobilized systems. The encapsulated systems demonstrated high activity and differentiated form of saccharifying the starch.

Graphical Abstract
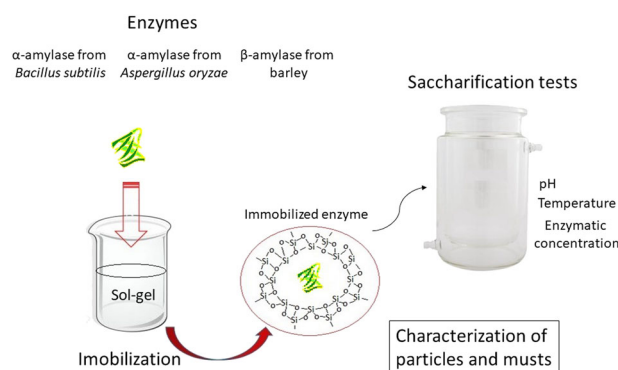
Highlights

- Catalytic activity of encapsulated amylase depends on the nature of amylase
- Optimum pH range of the immobilized enzymes was shifted to higher values
- Glucose to maltose ratio production is affected by the immobilization

✉ João H. Z. dos Santos
  jhzds@iq.ufrgs.br

[1] Departamento de Engenharia Química, Universidade Federal do Rio Grande do Sul Rua Eng. Luis Englert s/n, Porto Alegre, RS

90040-040, Brazil

[2] Instituto de Química, Universidade Federal do Rio Grande do Sul, Porto Alegre, RS, Brazil

1 Introduction

Amylase is an important amylolytic enzyme participating in the hydrolysis of starch, the most common carbohydrate in nature. Highly productive amylases for wider range of applications are still intensely investigated [1–3]. Amylase is an enzyme that catalyzes the breakdown of glycoside bonds of starch into simple sugars. Amylase plays an important role in the industrial application. These enzymes can be produced from plants, animals, and microorganisms [4]. The amylases are endoglucanases, which in the saccharification process of the starch produce low molecular weight compounds, such as glucose, maltose, and maltotriose.

Among the strategies to optimize the manipulation (separation and recovery) and to confer stabilization of enzymes, their immobilization on or within inert supports represents a very important field of research. Enzyme immobilization consists of the confinement of the enzyme within a phase (matrix/support) different from that of the substrates and/products. An ideal matrix must encompass characteristics, such as inertness, physical strength, stability, ability to increase enzyme specificity/activity and to reduce product inhibition, nonspecific adsorption and microbial contamination [5].

Inert polymers and inorganic materials are usually used as supports. Natural polymers such as chitosan can be used for the immobilization of enzymes [6]. Synthetic polymers such as polyaniline are also used to synthesize films with enzymes [7]. The use of an inorganic matrix has also been proposed for enzyme immobilization. For instance, alumina has been used to protect the enzymes from photodegradation [8].

Among the synthesis routes, the sol–gel process represents a potential technique for immobilizing or encapsulating labile enzymes within inorganic oxide matrices under mild conditions (low temperature and pressure) [9, 10]. In the routes based on metal alkoxydes, this process consists of the hydrolysis and co-condensation of tetraethyl orthosilicate (TEOS). The interaction between the encapsulated enzyme and the matrix network determines the degree to which the molecule retains its native properties [11].

The sol–gel process has already been used to encapsulate several enzymes, including lipase [12] cellobiase [13] and therapeutic enzymes [14]. Amylase has also already been immobilized by sol–gel process. For instance, immobilized α-amylase using sol–gel to generate a guar gum-gelatin-silica nanohybrid has been reported [15]. Immobilization of *Aspergillus oryzae* PP in order to enhance α-amylase activity is also described in the literature [16]. A simplified procedure for the preparation of immobilized β-amylase using nonpurified extract from fresh sweet potato tubers has been developed [17]. A carbon–silica carrier of α-amylase enzyme (of microbial nature) was synthetized [18]. Immobilized α-amylase enzymes in methyltriethoxysilane/tetraethoxysilane sol–gel matrices have also been investigated [19].

To the best of our knowledge, the effect of the nature of the amylase source on the performance of the resulting encapsulated systems in starch hydrolysis has not been reported. Thus, in the present investigation, we studied the comparative immobilization of amylase from *Bacillus subtilis*, α-amylase from *A. oryzae*, and β-amylase from barley within a silica-based matrix by acid-catalyzed sol–gel process. The resulting systems were characterized by a set of complementary techniques, namely, Fourier transform infrared spectroscopy (FT-IR), nitrogen adsorption, scanning electron microscopy (SEM), and small-angle X-ray scattering (SAXS). The immobilized enzymes were evaluated in starch hydrolysis under different reaction conditions (catalyst amount, pH, and temperature).

There are several studies that document the entrapment of enzymes via sol–gel, but most of them analyze a single type of enzyme, in some cases two ones. What differentiates this research from the others is the comparative analysis of three enzymes of different origins (bacterial, fungic, and vegetal) submitted to the respective reactional conditions of the optimal ones. This allows us to make comparisons that would not be plausible when comparing different academic works where the biocatalytic systems are differentiated.

2 Experimental procedure

2.1 Materials

Enzymes α-amylase from *B. subtilis*, α-amylase from *A. oryzae*, and β-amylase from barley were purchased from Sigma-Aldrich. For the sol–gel synthesis, the following reagents were employed: isopropyl alcohol (99.5%-Dinâmica), TEOS (98%-Sigma-Aldrich), buffer solution (aqueous solution containing $CaCl_2$ and sodium acetate), hydrochloric acid and water. Phenol (99%-Dinâmica) and potassium tartrate (99%-Dinâmica), sodium metabisulfite (97%-NEON), dinitrosalicyclic acid (98%-Sigma-Aldrich), citric acid (99.5%-NEON), and sodium bibasic phosphate (98%-NEON) were used in the DNS method. Soluble starch (99%-Dynamic) was used. Glucose and maltose standards used for HPLC were also purchased from Sigma-Aldrich.

2.2 Enzyme immobilization

For the immobilization of the amylases within the silica matrices, the sol–gel acid-catalyzed process was employed. In a typical preparation, 5 mL of TEOS, 3 mL of isopropyl alcohol, 20 mL of deionized water, 1 mL HCl (0.01 N), and

0.35 mL buffer solution (sodium acetate and $CaCl_2$) were added into a beaker under constant stirring at 60 °C. The amount of enzyme (0.5, 2, or 5 mg) was previously diluted in a buffer solution. After a given time (1, 2, or 3 h), the reaction medium temperature was reduced to 50 and 45 °C (still in absence of of α-amylase and beta-amylase), since protein denaturation takes place at 60 °C. In the case of bacterial α-amylase, this temperature reduction was not necessary, since its operating temperature is higher. Then, 2 mL of the buffer solution (control pH denaturation) and the diluted enzyme solution (less than 1 mL) were added. The system was left under stirring for 30 additional minutes. Gelling occurred sooner than 4 h from the beginning of the reaction.

The labels used to represent the immobilized enzymes consists of three or two letters corresponding to the encapsulated enzyme and a number representing the amount of the enzyme added during the sol–gel synthesis. For example, αBA-10 represents the immobilization of 10 mg of the bacterial alpha-amylase enzyme. Similar labels were adopted for fungal alpha-amylase (αFA) and beta-amylase (βA).

2.3 Characterization of the immobilized enzymes

Before characterizations, the resulting encapsulated enzymes were dried at 60 °C for 72 h.

2.3.1 Fourier transform infrared spectroscopy (FT-IR) and attenuated total reflection (ATR)

The infrared molecular absorption spectra of the supports were analyzed using the Shimadzu FTIR-8300 spectrophotometer with a DLaTGS detector (standard deuterated L-alaninedopedtriglycine sulfate), in the range of 2000–400 cm^{-1} with the resolution of 4 cm^{-1}. The samples were mixed with dry KBr and analyzed as pellets. The samples were also analyzed using the ATR mode in which the sample powder was directly analyzed. For ATR analysis, an Alpha-P (Bruker) accessory was used with the diamond prism at 45° and the spectral resolution of 4 cm^{-1}. Twenty-four scans were performed and their results were averaged for each measurement.

2.3.2 Nitrogen adsorption (BET and BJH methods)

The surface area, size, and volume of the pores of the encapsulated enzymes were evaluated based on the nitrogen-adsorption-desorption isotherms obtained at −196 °C. Approximately 100–200 mg of dried sample was used. The samples were previously degassed at 110 °C for 18 h under vacuum in a MicromeriticsVacPrep 061 instrument. The physical nitrogen adsorption isotherms per sample were obtained using a MicromereticsTriStar II 3020 instrument in the partial pressure range of 0.01 < P/Patm < 0.25. The surface area (S_{BET}) was calculated by the Brunauer–Emmett–Teller method (BET), while the pore size and volume were obtained using the desorption isotherm according to the Barret–Joyner–Halenda method (BJH).

2.3.3 Scanning electron microscopy (SEM)

SEM experiments were carried out using a BOI-SEM-10 microscope. The samples were initially attached to a carbon tape and then coated with carbon by conventional spray techniques.

2.3.4 Small-angle X-ray scattering (SAXS) measurements

The SAXS experiments were carried out using synchrotron radiation at LNLS (Campinas, Brazil) with the wavelength λ = 0.1488 nm and the detector/channel ratio of 0.158. The samples were placed in stainless steel sample holders closed by Kapton® tape. The measurements were performed at two sample-detector distances of 672.48 and 2285.84 nm. The intensity was corrected considering the correct intensity of the incident ray, the absorption of the sample and the subtraction of the blank. Low- and high-angle data were merged using the Mathematic® software to generate an integrated file of each sample. Data analysis was performed using the Irena software [20], and the evaluation routine was implemented in the IgorPro program (WaveMetrics, Portland, USA) [21].

2.4 Evaluation of encapsulated enzyme catalytic activity in starch hydrolysis

Free and encapsulated enzymes were used for the starch hydrolysis reactions. All reactions described here were conducted in an outer jacketed glass reactor coupled to a water circulator that was used to control the temperature. The stirring speed was kept identical for all reactions.

The cooled enzyme was diluted in a buffer solution (buffer + $CaCl_2$), also refrigerated, in order to avoid the catalytic loss by thermal shock. This diluted enzyme underwent gradual warming up to its use.

The gradual heating temperatures of the diluted or immobilized enzymes were close to the saccharification temperatures of 60, 50, and 45 °C for the bacterial α-amylase, fungal α-amylase, and beta-amylase enzymes, respectively.

The suspension was made by diluting 0.0025 mol of sodium acetate, 0.0005 mol of $CaCl_2$, and 1 g of starch in a reaction volume of 100 mL using deionized water. Thereafter, the suspension underwent a pH adjustment, using acetic acid, NaOH, or sodium bicarbonate to adjust the pH.

In batch processes, a temperature of 65 °C was used for the bacterial α-amylase enzyme (*B. subtilis*), which was added to the reactor by the beginning of the reaction. The choice of this temperature relied on the fact the under such conditions, the process of liquefying the starch occurs in an efficient way. On the other hand, for α-amylase (*A. oryzae*) and β-amylase (barley) enzymes lower operating temperature (50 and 45 °C, respectively) were employed. Taking into account that the necessity to liquefy the starch, the reaction medium (suspension) was initially heated to 70 °C for 15 min and subsequent cooled. Once the operating temperature was reached, the enzyme was added.

All reactions were performed for 60 min. Then 0.5 mL aliquots were withdrawn. These were immediately heated in a water bath at 100 °C for 5 min to hinder enzyme activity, and then cooled to preserve the samples until the analysis of the reducing sugars (DNS method).

2.4.1 Methods of analysis of the resulting sugars

The quantitative determination of the reducing sugars was carried out according to the dinitrosalicylic acid (DNS) method developed by Miller [22]. A standard curve ($y = 0.3957 + 0.0099$, $R = 0.9914$, $N = 7$) was drawn upon measuring the absorbance at 540 nm.

2.4.2 High-performance liquid chromatography (HPLC)

Chromatographic analysis was performed using a Dionex Ultimate 3000 HPLC system equipped with a refractive index detector. The employed column was a BioRad Aminex® HPX-87H (300×7.8 mm $\times 9$ μm) at the temperature of 60 °C. The mobile phase consisted of 0.001 M sulfuric acid in the isocratic mode at the flow rate of 0.8 mL min^{-1}. The injection volume was 20 μL and the analysis time was 16 min. Standard curves of glucose ($y = 0.0035 + 0.0466$, $R^2 = 0.9991$, $N = 9$) and maltose ($y = 0.0034 + 0.0136$, $R^2 = 0.9989$, $N = 9$) were obtained. The performance of the resulting encapsulated systems was evaluated in terms of starch hydrolysis. For comparison, the free (nonencapsulated) systems were also evaluated.

3 Results and discussion

3.1 Effect of the addition time

The effect of the addition time of the enzyme on the resulting catalyst activity is illustrated in Table 1, showing the reducing sugars amount results using encapsulated α-amylase in which the enzyme was added at different times from the beginning of the reactions.

Table 1 Effect of addition the time of bacterial α-amylase during sol–gel synthesis on the production of reducing sugars

Enzyme	Addition time (hour)	Reducing sugars (μmol/mL)
α-amylase (*Bacillus Subtilis*)	1	≈0
	2	19.9
	3	27.4

Catalyst amount: 5 mg; temperature: 65 °C; pH: 6.0

According to Table 1, after 3 h from the beginning of the sol–gel process, the reaction medium has acquired low levels of denaturing compounds of the enzymes affording more active catalyst systems. It is worth noting that after 4 h from the beginning of the reaction, the material is completely gelled, so it is therefore impossible to add the enzyme solution. Thus, the enzyme addition time of 3 h to the sol–gel reaction medium was adopted for the further encapsulated-enzyme systems. It cannot be overlooked that the addition time of the enzyme may affect its distribution within the particle core. The distribution of the enzyme closer to the particle center is enhanced with the earlier addition of the enzyme, which in turn may affect the accessibility of the enzyme to the catalytic reaction.

3.2 Effect of catalyst amount

Figure 1 presents the results for the concentrated reducing sugars for free and encapsulated enzymes using several catalyst concentrations. Optimum temperatures and pH were employed according to the literature [23–25].

According to Fig. 1, the free enzymatic systems presented higher activity than the immobilized systems. Such behavior is intrinsic to supported/immobilized catalysts, in which a decrease is observed when comparing homogeneous (free) and immobilized systems. In the former, the enzyme is more easily accessed by the reagents, while in the case of immobilized (heterogeneous) systems, the surface plays the role of a bulky ligand hampering the access of the reagents to the catalyst center.

The concentration and biocatalytic activity show a positive correlation. Furthermore, bacterial α-amylase from *B. subtili*s and fungal α-amylase from *A. oryzae* showed maximum conversions very close to one another, at above 30 μmol/mL in the free systems. β-amylase had lower conversion values (below 30 μmol/mL).

Considering the free systems (Fig. 1), it is noted that the systems containing bacterial α-amylase from *B. subtilis* showed sensitivity in the range of the used concentration. On the other hand, the fungal α-amylase from *A. oryzae* and β-amylase presented close values which shows less susceptibility as the enzyme concentration parameter changes.
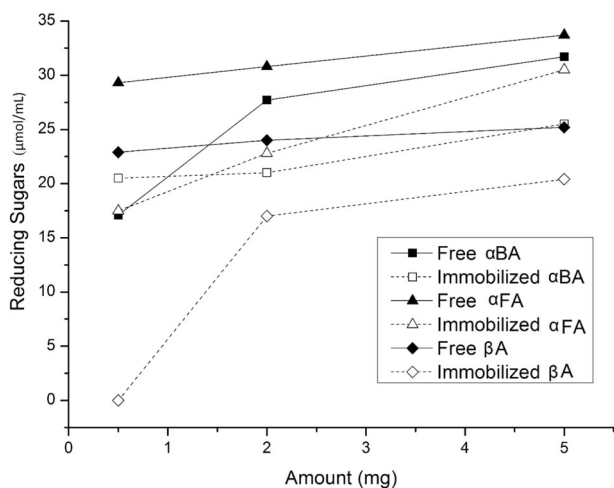
Fig. 1 Concentration of reducing sugars obtained from free and immobilized systems. Conditions: free and immobilized αBA (T = 65 °C, pH = 6.0); free and immobilized αFA (T = 50 °C, pH = 5.3); free and immobilized βA (T = 50 °C, pH = 5.3)

Table 2 Effect of the concentration of reducing sugars produced for the free- and encapsulated systems under optimal and varied pH reaction conditions

Enzyme	Amount (mg)	pH	T (°C)	$C_{\text{free enzymes}}$ (μmol/mL)	$C_{\text{immobilization enzymes}}$ (μmol/mL)
αBA	**2**	**6.0**	**65**	**27.7**	**21.0**
	2	7.0	65	25.1	18.2
	2	5.0	65	23.7	18.4
	5	**6.0**	**65**	**31.7**	**25.5**
	5	7.0	65	26.0	20.9
	5	5.0	65	23.2	13.6
αFA	**2**	**5.3**	**50**	**30.8**	**22.8**
	2	6.3	50	28.3	22.1
	2	4.3	50	11.7	14.5
	5	**5.3**	**50**	**33.7**	**30.5**
	5	6.3	50	30.6	30.8
	5	4.3	50	14.2	15.1
βA	**2**	**5.25**	**45**	**24.0**	**17.0**
	2	6.25	45	18.8	14.5
	2	4.25	45	14.4	traces
	5	**5.25**	**45**	**25.2**	**20.4**
	5	6.25	45	25.1	21.9
	5	4.25	45	13.7	9.4

Bold values indicates the optimized chosen condition

Among the immobilized systems, beta-amylase showed the highest sensitivity to the concentration variation.

3.3 Effect of the pH

Reactions were performed at higher and lower pH compared with those initially analyzed (optimal values according to the literature). Table 2 shows the conversions obtained by varying the reaction pH.

According to Table 2, conversion to reducing sugars at lower pH appears to be greatly affected for fungal α-amylase and β-amylase. This effect of acid pH is more subtle in the case of bacterial α-amylase.

On the other hand, the encapsulated systems appears to be less affected by pH, showing very close conversion among the investigated pH values: (i) in the case of bacterial α-amylase at the three analyzed pH; (ii) in the case of fungal α-amylase at two pH (6.3 and 5.3); and (iii) in the case of β-amylase at two pH (6.3 and 5.3). This shows greater stability with respect to pH variation.

The activity of the β-amylase enzyme at pH 4.25 is quite low suggesting that encapsulated enzymes have a tendency to perform better at higher pH. The optimal activity range of an encapsulated enzyme appears to be shifted to higher values. These results corroborated the literature reports of an increase in the catalyst activity from pH 5.6 (free enzyme) to 6.0 (encapsulated enzyme) for the encapsulation of α-amylase via the sol–gel process [19].

3.4 Effect of reaction temperature

Several reactions were carried out at higher temperatures to evaluate the performance of the enzymes in the hydrolysis of starch at different temperatures. Table 3 presents the results of these experiments.

As shown in Table 3, increasing temperature affected the free systems differently: for the α-amylase, a decrease in the conversion (a single exception) was observed, while for beta-amylase an increase in the conversion was detected. α-amylase immobilized systems also presented lower conversion at higher temperatures (one exception). Immobilized β-amylase exhibited similar conversions at different temperatures.

This decrease in the conversion of immobilized systems with the temperature is in disagreement with the data reported in the literature [26], where it was found that increasing the reaction temperature from 50 °C to 70 °C resulted in an increase in the conversion of starch hydrolysis using bacterial α-amylase (*B. subtilis*).

The immobilized systems were further characterized by a series of complementary techniques, as discussed in the following sections.

3.5 Characterization of the immobilized systems

Figure 2 shows the FT-IR spectra of the free bacterial α-amylase enzyme and the comparison of this encapsulated enzyme in silica. For comparison, the silica spectrum was

Table 3 Effect of the concentration of reducing sugars produced for the free- and encapsulated systems under optimal and varied temperature reaction conditions

Enzyme	Amount (mg)	pH	T (°C)	$C_{\text{free enzymes}}$ (µmols/mL)	$C_{\text{immobilization enzymes}}$ (µmols/mL)
αBA	**0.5**	**6.0**	**65**	**17.1**	**20.5**
	0.5	6.0	70	19.8	15.5
	5	**6.0**	**65**	**31.7**	**25.5**
	5	6.0	70	23.3	20.6
	5	6.0	75	22.4	19.2
αFA	**0.5**	**5.3**	**50**	**29.3**	**17.5**
	0.5	5.3	55	16.2	18.9
	5	**5.3**	**50**	**33.7**	**30.5**
	5	5.3	55	27.2	27.7
βA	**2**	**5.25**	**45**	**24**	**17.0**
	2	5.25	50	28.4	17.0
	5	**5.25**	**45**	**25.2**	**20.4**
	5	5.25	55	28.5	20.8

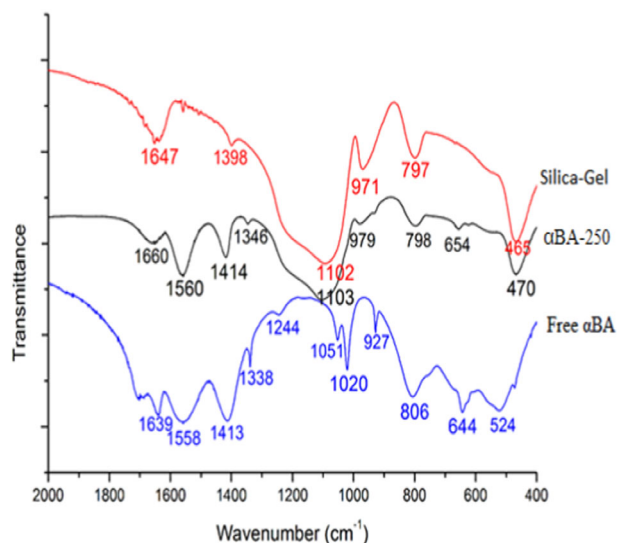Bold values indicates the optimized chosen condition

Fig. 2 FT-IR spectra (transmission mode) of free and immobilized bacterial α-amylase enzyme. For comparative reasons, silica spectrum was also included

also included. The main peaks are reported and assigned in Table 4.

According to Fig. 2, the most intense peaks from the free enzyme can be observed in the resulting encapsulated systems. Examination of the spectra presented in Fig. 2 and the peaks assigned in Table 4, shows that the band centered at 1660 cm^{-1} in the FT-IR of the immobilized bacterial α-amylase exhibited the largest wavenumber shift in comparison to that of the free enzyme. This band is associated

with the N–H stretching from folding in primary amines, which in the free system has a broad band centered at 1639 cm^{-1}. The interaction of these groups is also observed through the 10 cm^{-1} wavenumber shift observed by the comparison of the 644 cm^{-1} (free) and 654 cm^{-1} (immobilized) frequencies of the enzymes. This band is assigned to the angular N–H deformation outside the plane. These results suggest that the interaction between enzyme and silica network occur through the interaction between the amine moieties and silanol groups.

The peak associated with $\nu_{\text{(C–N)}}$ of the tertiary amides and the N–H deformation (1338 cm^{-1} in the free enzyme) also exhibited a significant wavenumber shift in the encapsulated systems (1346 cm^{-1}), suggesting the interaction between the enzyme and the silica framework may occur through these group. It is worth noting that the small peak detected in the silica spectrum at 1398 cm^{-1} (C–H bending) may be due to the residual ethyl groups (from TEOS) which may remain in the silica structure, as assigned in the literature [27].

It is worth noting that in the case of the two other encapsulated enzymes (αFA-250 and βA-250), the differences in the peak centered at 970 cm^{-1} (associated to Si–O–Si angular deformation) suggest that the nature of the enzymes may affect the internal organization of the silica framework.

The results for the systems obtained in the transmission and reflectance modes were comparatively analyzed. It is important to explain that while in the transmission mode the entire sample is analyzed by the incident beam (bulk and surface), in the ATR mode, only the uppermost surface region is analyzed.

In fact, the use of both modes of infrared spectroscopy aimed at getting information about the sample distribution between the more external layers (ATR) and the bulk (absorption/transmission modes provides information of the bulk and of the surface, since the radiation cross the simple). In ATR mode, the light is not reflected directly on the boundary surface but by a virtual layer the fraction of light wave that reaches into the samples (evanescent wave). Therefore, the sampling in the case of ATR is richer in information on the externa layers of the particles

The comparison of the band intensities between two modes may provide some insight about the components distribution along the particle grains. Band area was normalized to the most intense Si–O large band centered ca. 1100 cm^{-1} as illustrated in Table 5).

Analysis of the ATR and FT-IR spectra of αBA shows that the peak located at 1554 cm^{-1} (ATR)–1560 cm^{-1} (FT-IR) demonstrates a distinct nonunity relative ratio between ATR and FT-IR results: 1554 cm^{-1} (10.3%) in ATR and 1560 cm^{-1} (17.2%) in FT-IR. Such results suggest that the enzyme may be distributed more within the particle rather

Table 4 FT-IR peaks assignement according to [31, 32]

Infrared Band (cm^{-1})			Assignment
Silica	Free bacterial α-amylase	Immobilized bacterial α-amylase	
1647	1639	1660	N–H angular deformation outside plane
–	1558	1560	NH bending and CN stretching
1398	1413	1414	C–H bending
–	1338	1346	C–N stretching of the tertiary amides and the N–H deformation
1102	–	1103	Asymmetrical Si–O stretching
971	–	979	Angular Si–O–Si deformation
–	806	–	Symmetrical N–H angular deformation
797	–	798	Symmetrical Si–O stretching
–	644	654	Angular N–H deformation outside plane
465	–	470	Si–O–Si deformation

Table 5 Results obtained by the area analysis of the ATR and FT-IR peaks from αBA

Peak (cm^{-1})		Relative value (%)—ATR	Relative value (%)—FT-IR
ATR	FT-IR		
1554	1560	10.3	17.2

than on the surface. Therefore, this difference shows that there is some difference in the distribution of the enzyme in this sample.

3.6 Surface area and porosity

Figure 3 presents the nitrogen adsorption isotherms of the resulting xerogels. The silica gel showed a type IV isotherm with a hysteresis loop, which are typical for mesoporous solids and are usually associated with pores with narrow necks and wide bodies according to the literature [28].

Textural characteristics of the three encapsulated enzymes were evaluated in the three investigated concentrations, for a total of nine encapsulated systems in addition to the silica gel. For comparison, data from the bare silica were also included (Table 6).

According to Table 6, all encapsulated enzymes had high surface area above 300 m^2/g. The synthesis without the presence of enzyme (silica gel) results in a larger surface area (508 m^2/g) with the exception of the βA-2.5 and βA-25 systems, which presented higher surface area (538 and 554 m^2/g, respectively). Therefore, it is plausible to assume that the presence of the enzyme in the sol–gel process reduces the surface area. The resulting surface areas are higher than those reported in the literature for the sol–gel encapsulation of lipases (224 m^2/g).

The pore volume appears to vary independently of the enzyme concentration, with values in the range of 0.46–0.81 cm^3/g. The pore diameter appears to be slightly positively correlated with the enzyme concentration, varying in the range of 32.0–89.6 Å.

Analysis of mesoporous silicas has suggested that enzymes are deposited within the pores. It is worth mentioning that the knowledge on the changes during immobilization and the microenvironment in which the enzyme is confined is essential for evaluating catalytic activity [29]. In the case of this immobilization via sol–gel, it seems that the enzyme migrates into the particles, since the addition of the enzyme is late and the ATR analyses suggest a higher enzyme concentration inside the particles., This altered environment may explain the difference in activity between the free and immobilized enzymes observed in the present study.

Strong Spearmen correlation ($r_{Sp} = 0.951$) between the pore diameter and catalyst activity was observed, suggesting that this characteristic is probably very important for the substrate and products diffusion.

3.7 Scanning electron microscopy (SEM)

The morphology of the obtained systems was evaluated by SEM. The visual analysis of the obtained images allows the identification of two kinds of structures, namely, the less spherical structures and more granular object, suggesting spherical structures, as illustrated in Fig. 4.

The granular structure was predominant in the samples, which can be considered an advantage of this technique, because granular structures should have a higher surface porosity. The samples were composed of large clusters of porous particles providing higher porosity to the immobilized samples as shown in Fig. 4a. This could explain
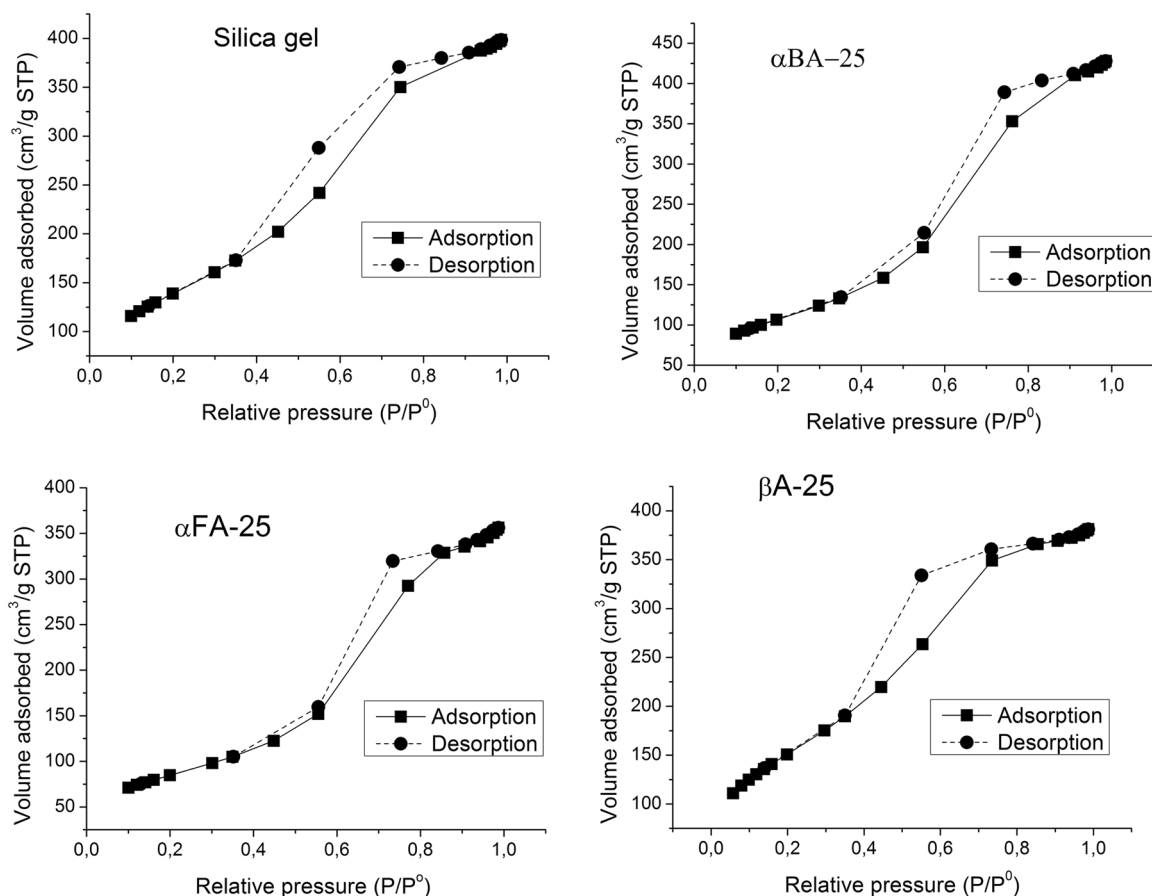
Fig. 3 The nitrogen adsorption/desorption isotherms of resulting xerogels

Table 6 Textural characteristics of the encapsulated systems

Symbol	BET surface area (m^2/g)	Pore volume BJH desorption (cm^3/g)	Pore diameter BJH desorption (Å)
Silica gel	508	0.65	36.6
αBA-2.5	474	0.64	36.7
αBA-10	139	0.46	89.6
αBA-25	391	0.67	45.2
αFA-2.5	337	0.47	32.8
αFA-10	456	0.52	31.6
αFA-25	310	0.56	48.8
βA-2.5	538	0.60	32.2
βA-10	437	0.81	50.9
βA-25	554	0.63	32.0

the high efficiency of some immobilized enzymes. Studies reported in the literature analyzing the micrographs of pure silica gel reported the presence of a rigid surface structure that most likely forms only one block. Addition of the enzyme and Aliquat 336 (a liquid hydrophobic material) induced a modification in the morphology of the silica sol–gel. The resulting biocatalyst morphology

presented a surface bearing greater roughness with more rounded shapes, although pores were still irregular according to the literature [12].

3.8 Small-angle X-ray scattering (SAXS) measurements

Table 7 shows the results obtained using SAXS. All samples showed three levels.

According to Table 7, the size of the primary particle (Rg1) appears not to be affected by whether or not the encapsulated enzymes are present, because its value does not exhibit significant difference between the systems consisting of bare silica and those containing the encapsulated enzyme. Similar behavior could be observed in the case of the secondary particle size (Rg2). The second and third levels are obtained by the power-law scattering exponent (P) from the decay of the scattering curve. This decay is indicative of the fractal dimension of these particles or clusters, which, in this case, provides information regarding the surface. If the P value is between 1 and 3, the structure will be a mass fractal, which means that the branched structure is similar to a polymer. If the P value is

Fig. 4 a Granular structures visualized by SEM. Image obtained from sample βA-10. **b** Less spherical structures visualized by SEM. Image obtained from sample αFA-2.5
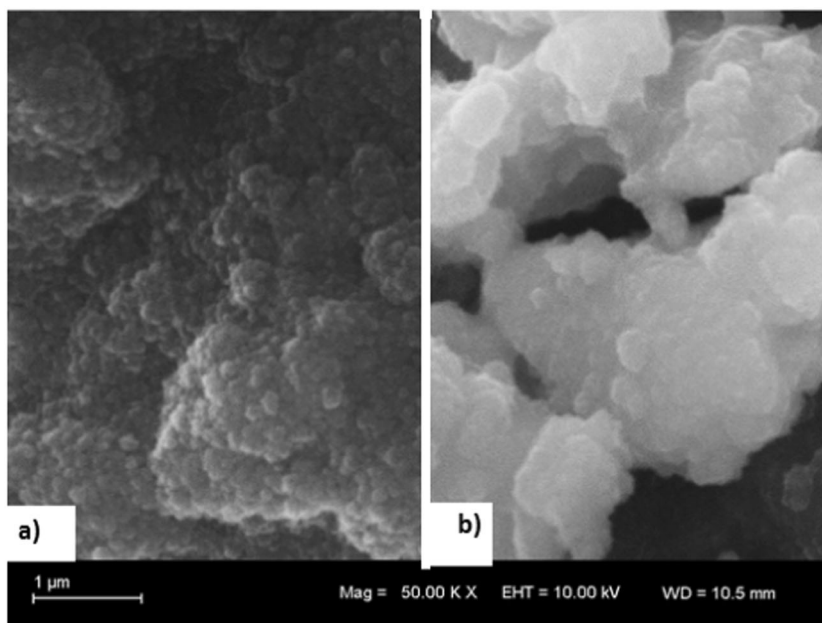

Table 7 SAXS parameters determined for the encapsulated systems

	Rg1 (nm)	P2	Rg2 (nm)	P3
Sílica gel	0.99	3.72	3.62	3.29
αBA-2.5	1.00	3.89	3.57	3.21
αBA-10	0.84	3.92	5.44	3.33
αBA-25	1.10	4.00	3.41	3.36
αFA-2.5	0.85	4.00	3.18	3.41
αFA-10	0.85	4.00	3.21	3.43
αFA-25	1.01	4.00	3.57	3.26
βA-2.5	0.95	3.04	3.86	3.31
βA-10	1.17	4.00	3.63	2.77
βA-25	0.98	3.07	3.87	3.39

Table 8 Glucose and maltose concentrations measured by HPLC produced by free systems

Enzyme	pH	T (°C)	Free System	
			Glucose (mg/L)	Maltose (mg/L)
αBA	5.0	65	537	1607
	6.0	**65**	**1245**	**3031**
	7.0	65	544	1593
αFA	4.3	50	67	2502
	5.3	**50**	**408**	**5501**
	6.3	50	291	5339
βA	4.3	45	46	5669
	5.3	**45**	**69**	**5011**
	6.3	45	140	7467

Amount: 5 mg

Bold values indicates the optimized chosen condition

between 3 and 4, the structure will be a fractal surface, i.e., dense in the core but roughened on the outer surface. For a *P* value equal to or greater than 4, a dense material with a smooth and uniform surface is formed. The calculated *P* values are shown in Table 7, and it can be seen that all solids exhibited *P* values ranging roughly from 3.0 to 4.0. Thus, we have dense, spherical and uniform particles with a slightly rough surface for all materials.

It is worth noting that the values of the P2 and P3 coefficients suggest a structure closer to the mass fractal moieties. A negative Spearmen correlation ($r_{Sp} = -0.953$) between P3 and catalyst activity is found, suggesting that the more compact the structure, the lower its catalyst activity.

3.9 Selectivity in starch hydrolysis

The selectivity of the encapsulated systems in starch hydrolysis was evaluated in terms of glucose and maltose production. Table 8 presents the results obtained from HPLC measurements for the free (nonencapsulated) systems at different adjusted pH values.

According to the data in Table 8, for the free (nonencapsulated) systems, it is worth noting that the three employed enzymes generated a higher concentration of maltose than glucose. Among the three investigated enzymes, bacterial α-amylase showed the highest concentration of glucose and the lowest concentration of maltose.

Fungal α-amylase resulted in reactions with glucose concentrations in the range of 67–408 mg/L while for maltose the reactions occurred in the range of 2502–5501 mg/L. β-amylase had one with the highest concentrations of maltose and lowest concentrations of glucose, clearly showing that their free systems produce a much higher rate of maltose in relationship to glucose, which is in agreement with the basic biochemical literature that affirms the unique production of maltose from β-amylase [30].

Table 9 Estimated glucose and maltose concentrations obtained by HPLC for the encapsulated systems

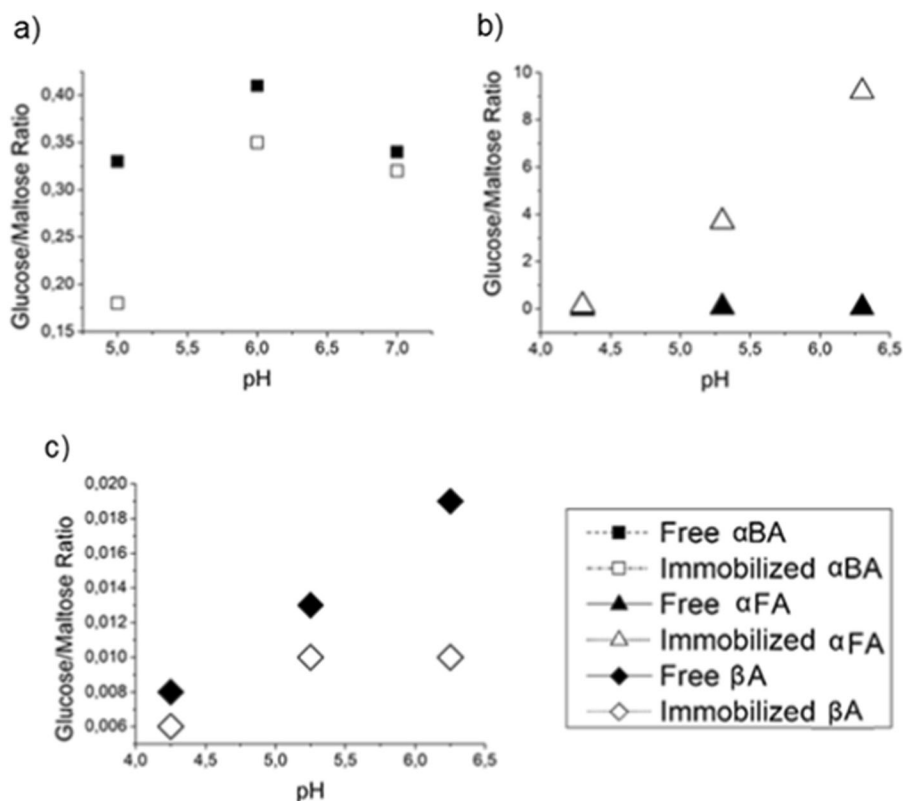| Enzyme	pH	T (°C)	Immobilized systems	
			Glucose (mg/L)	Maltose (mg/L)
αBA	5.0	65	276	1534
	6.0	**65**	**386**	**1105**
	7.0	65	367	1140
αFA	4.3	50	290	2116
	5.3	**50**	**85.4**	**22.8**
	6.3	50	157	17
βA	4.3	45	21.2	3494
	5.3	**45**	**21.7**	**1817**
	6.3	45	83.7	8279

Table 9 shows the production of glucose and maltose from starch hydrolysis by the encapsulated systems.

The glucose and maltose concentrations of the immobilized systems are lower than those of the respective free systems with some exceptions. However, the systems using fungal α-amylase had a very low maltose concentration at pH 5.3 and 6.3, which resulted in a well-differentiated glucose/maltose ratio.

It is worth mentioning that an inverse Spearmen correlation ($r_{Sp} = -0.807$) was observed between the glucose/maltose ratio and the BET surface area. This suggests that the encapsulation within the silica matrix may affect the enzyme configuration which in turn may tune the sugar ratio production.

According to the data presented in Tables 8, 9, the pH appears to affect the amount of glucose and maltose, as shown in Fig. 5.

In the free systems from bacterial α-amylase, the different pH used during the reactions affect glucose and maltose concentrations, but the glucose/maltose ratio appears to remain relatively stable, varying in the range of 0.33–0.41.

The immobilized systems that used bacterial α-amylase had a higher maltose to glucose ratio (which had already occurred in the free systems). The ratio of these sugars was in the range of 0.18–0.35, slightly lower than that obtained by the analogous free systems that showed a glucose/maltose ratio in the range of 0.33–0.41.

Fig. 5 Glucose/Maltose ratio versus pH **a** αBA, **b** αFA, and **c** βA

In the free systems, fungal α-amylase showed an intermediate glucose concentration and a high maltose concentration. The glucose/maltose ratio appears to remain relatively stable, ranging from 0.026 to 0.074, which in turn is much closer to that obtained using β-amylase than to that of bacterial α-amylase.

Immobilized fungal α-amylase systems at pH 5.3 and 6.3 presented ratios of 3.7 and 9.2, respectively, which are very different from the ratios for their respective free systems. The encapsulated batch using pH 4.3 presented a much more similar relation to the free system. Therefore, the results obtained at different pH using immobilized fungal α-amylase demonstrated a large difference.

The glucose/maltose ratio obtained from beta-amylase is very close to 0 for both the free and immobilized systems.

4 Conclusion

Immobilized β-amylase (from barley) presented conversions lower than those of its respective free systems, suggesting that it is an enzyme which is more prone to deactivation when subjected to the encapsulation in the acid-catalyzed sol–gel process. The immobilized α-amylase from *B. subtilis* and α-amylase from *A. oryzae* also showed lower conversions, but the drop in activity was more subtle. Therefore, they appear to be more robust enzymes and much more resistant after the sol–gel encapsulation process. In the investigated systems, the optimum pH range of the immobilized enzymes was shifted to higher values compared with the free enzymes. For the product conversion, the glucose to maltose ratios of the immobilized α-amylase (fungic) enzyme were very different from the ratios for their respective free system, which suggests that the encapsulation strongly affected the mechanism of this enzyme's action in starch degradation.

Compliance with ethical standards

References

1. Talekar S, Joshi A, Kambale S, Jadhav S, Nadas S, Ladole M (2017) A tri-enzyme magnetic nanobiocatalyst with one pot starch hydrolytic activity. Chem Eng J 325:80–90

2. Chen Y, Liu H, Zheng X, Wang X, Wu J (2017) New method for enhancement of bioenergy production from municipal organic wastes via regulation of anaerobic Zermentation process. Appl Energy 196:190–198

3. Sorndech W, Sagnelli D, Blennow A, Tongta S (2017) Combination of amylase and transferase catalysis to improve IMO compositions and productivity. Food Sci Technol 79:479–486

4. Kathiresan K, Manivannan S (2006) α-Amylase production by *Penicillium fellutanum* isolated from mangrove rhizosphere soil. Afr J Biotechnol 5:10

5. Singh BD (2009) Biotechnology expanding horizons. Kalyani, India

6. Sfahair ZU, Ningsh DR, Kartika D, Zuliana AL (2017) *Bacillus thuringiensis* HCB6 amylase immobilization by chitosan beads. OP Conferences Series: Mater Sci Eng 172:1–10

7. Singh S, Saikia JP, Buragohain AK (2013) A Novel reusable PAni-PVA-Amylase film: activity and analysis. Coll Surf, B 106:46–50

8. Shapovalova OE, Levy D, Avnir D, Vinogradov VV (2016) Protection of enzymes from photodegradation by entrapment within alumina Coll Surf B Biointerfaces 146:731–736

9. Matsui K (2005) Entrapment of Organic Molecules. In: H Kosuka (ed) Handbook of Sol–Gel Science and Technology: Process. The Neterlands: Springer

10. Ciriminna R, Fidalgo A, Pandarus V, Béland F, Ilharco LM, Pagliaro M (2013) The Sol–gel route to advanced silica-based materials and recent applications. Chem Rev 113:6592–6620

11. Jin W, Brennan JD (2002) Properties and applications of proteins encapsulated within sol–gel derived materials. Anal Chim Acta 461:1–36

12. Souza RL, Resende WC, Barão CE, Zanin GM, Castro HF, Santos OAA, Fricks AT, Figueiredo RT, Lima AS, Soares CMF (2012) Influence of the use of Aliquat 336 in the immobilization procedure in sol–gel of lipase from Bacillus sp. ITP-001. J Mol Catal B: Enzym 84:152–159

13. Das S, Berke-Schessel D, Hai-Feng, McDonough J, Wei Y (2011) Enzymatic hydrolysis of biomass with recyclable use of cellobiase enzyme immobilized in sol–gel routed mesoporous silica. J Mol Catal B: Enzym 70:49–54

14. Vinogradov VV, Avnir D (2014) Exceptional thermal stability of therapeutic enzymes entrapped in alumina sol–gel matrices. J Mater Chem B 2:2868–2873

15. Singh V, Singh D (2014) Diastase α-amylase immobilization on sol–gel derived guar gum-gelatin-silica nanohybrid. Adv Mater Lett 5:17–23

16. Evstatieva Y, Yordanova M, Chernev G, Ruseva Y, Nikolova D (2014) Sol–gel immobilization as a suitable technique for enhancement of α-amylase activity of *Aspergillus oryzae* PP. Biotechnol Biotechnol Equip 28:728–732

17. Tavano OL, La-Fuente RF, Goulart AJ, Monti R (2013) Optimization of the immobilization of sweet potato amylase usingglutaraldehyde-agarose support. Characterization of the immobilized enzyme. Process Biochem 48:1054–1058

18. Petrov AL, Erankin SV, Petrov LA, Shishmakov AB (2012) Sol–Gel Synthesis of an organic–inorganic composite for preparation of an active carrier of α-amylase. Glass Phys Chem 38:105–108

19. Vlad-Oros B, Oniga O, Dudas Z, Dragomirescu M, Preda G, Chiriac A (2007) Performance of immobilized bacterial alpha-amylase in methyltriethoxysilane/tetraethoxysilane sol–gel matrices. Ser Chem 16:261–266

20. Ilavsky J, Jemian PR (2009) Irena: tool suite for modeling and analysis of small-angle scattering. J Appl Crystallogr 42:347–353

21. Kline SR (2006) Reduction and analysis of SANS and USANS data using IGOR Pro. J Appl Crystallogr 39:895–900

22. MILLER GL (1959) Use of dinitrosalicylic acid reagent for determination of reducing sugar. Anal Chem 31:426

23. Femi-Ola TO, Olowe BM (2011) Characterization of alpha amylase from *Bacillus subtilis* BS5 isolated from *Amitermes evuncifer* Silvestri. Res J Microbiol 6:140–146

24. Sivaramakrishnan S, Gangadharam D, Nampoothiri KM, Soccol CR, Pandey A (2007) Alpha amylase production by *Aspergillus oryzae* employing solid-state fermentation. J Sci Ind Res 66:621–626

25. Mawahib EM, Yagoub SO (2010) Partial purification and characterization of α and β amylases isolated from Sorghum bicolor cv. (Feterita) Malt. J Appl Sci 10:1314–1319

26. Konsoula Z, Liakopoulou-Kyriakides M (2006) Starch hydrolysis by the action of an entrapped in alginate capsules α-amylase from *Bacillus subtilis*. Process Biochem 41:343–349

27. Nassor ECO, Ávila LR, Santos P, PF, Ciuffi KJ, Calefi PS, Nassar EJ (2011) Influence of the hydrolysis and condensation time on the preparation of hybrid materials. Mater Res 14:1–6

28. Thommes M, Kaneko K, Neimark AV, Olivier JP, Rodriguez-Reinoso F, Rouquerol J, Sing KSW (2015) Physisorption of gases, with special reference to the evaluation of surface area and pore size distribution (IUPAC Technical Report). Pure Appl Chem 87:1051–1069

29. Carlsson N, Gustafsson H, Thörn C, Olsson L, Holmberg K, Åkerman B (2014) Enzymes immobilized in mesoporous silica: A physical–chemical perspective. Adv Colloid Interface Sci 205:339–360

30. Lehninger DN, Cox, MM (2014) Principles of biochemistry. 6 ed, Artmed, Porto Alegre

31. Colthup L, Daly L, Wiberley S (1990) Introduction to Infrared and Raman Spectroscopy. 3 ed, Academic Press, San Diego

32. Vansant EF, Van Der Voor P, Vrancken KC (1995) Characterization and Chemical Modification of the Silica Surface. Elsevier, Amsterdam